Lawrence Berkeley National Laboratory

Title

Search for long-lived particles decaying to jet pairs

Authors

Aaij, R
Adeva, B
Adinolfi, M
et al.

Peer reviewed

THE EUROPEAN
PHYSICAL JOURNAL C

CrossMark

Search for long-lived particles decaying to jet pairs

LHCb Collaboration[*]

CERN, 1211 Geneva 23, Switzerland

Abstract A search is presented for long-lived particles with a mass between 25 and 50 GeV/c^2 and a lifetime between 1 and 200 ps in a sample of proton–proton collisions at a centre-of-mass energy of $\sqrt{s} = 7$ TeV, corresponding to an integrated luminosity of 0.62 fb^{-1}, collected by the LHCb detector. The particles are assumed to be pair-produced by the decay of a standard model-like Higgs boson. The experimental signature of the long-lived particle is a displaced vertex with two associated jets. No excess above the background is observed and limits are set on the production cross-section as a function of the long-lived particle mass and lifetime.

1 Introduction

A variety of models for physics beyond the standard model (SM) feature the existence of new massive particles whose coupling to lighter particles is sufficiently small that they are long-lived. If these massive particles decay to SM particles and have a lifetime between approximately 1 ps and 1 ns, characteristic of weak decays, they can be identified by their displaced decay vertex. Examples of such particles are the lightest supersymmetric particle in SUSY models with baryon or lepton number violation [1–4], the next-to-lightest supersymmetric particle in gravity mediated SUSY [5] and the neutral π_v particle in hidden valley (HV) models with a non-abelian gauge symmetry [6–8]. The latter model is particularly interesting as it predicts that experimental studies have sensitivity to the production of long-lived particles in SM Higgs decays.

This paper reports on a search for π_v particles, pair-produced in the decay of a SM-like Higgs particle with a mass of 120 GeV/c^2, close to the mass of the scalar boson

discovered by the ATLAS and CMS experiments [9,10].[1] The π_v candidates are identified by two hadronic jets originating from a displaced vertex. The vertex is required to be displaced from the proton–proton collision axis by more than 0.4 mm and less than 4.8 mm. The lower bound is chosen to reject most of the background from heavy flavour decays. The upper bound ensures that vertices are inside the LHCb beam pipe, which generates a sizeable background of hadronic interaction vertices. The signal is extracted from a fit to the di-jet invariant mass distribution. The analysis is sensitive to a π_v particle with a mass between 25 and 50 GeV/c^2 and a lifetime between 1 and 200 ps. The lower boundary on the mass range arises from the requirement to identify two hadronic jets while the upper boundary is mostly due to the geometric acceptance of the LHCb detector.

This analysis uses data collected in proton–proton (pp) collisions at a centre-of-mass energy of $\sqrt{s} = 7$ TeV. The data correspond to an integrated luminosity of 0.62 fb^{-1}, collected during the second half of the year 2011 when an analysis-specific trigger selection was implemented. Although similar searches have been reported by the CDF [11], D0 [12], ATLAS [13] and CMS [14] experiments, LHCb has a unique coverage for long-lived particles with relatively small mass and lifetime, because its trigger makes only modest requirements on transverse momentum.

2 Detector description

The LHCb detector [15] is a single-arm forward spectrometer covering the pseudorapidity range $2 < \eta < 5$, designed for the study of particles containing b or c quarks quarks. The detector includes a high-precision tracking system consisting of a silicon-strip vertex detector surrounding the pp interaction region [16], a large-area silicon-strip detector located upstream of a dipole magnet with a bending power of about

---

[*] e-mail: veerle.heijne@cern.ch

---

[1] The results are equally valid for a Higgs particle with a mass up to 126 GeV/c^2 within a few percent.

4 Tm, and three stations of silicon-strip detectors and straw drift tubes [17] placed downstream of the magnet. The tracking system provides a measurement of momentum, p, with a relative uncertainty that varies from 0.4 % at low momentum to 0.6 % at 100 GeV/c. The minimum distance of a track to a primary vertex, the impact parameter, is measured with a resolution of $(15 + 29/p_T)\,\mu$m, where p_T is the component of p transverse to the beam, in GeV/c. Different types of charged hadrons are distinguished using information from two ring-imaging Cherenkov detectors [18]. Photon, electron and hadron candidates are identified by a calorimeter system consisting of scintillating-pad and preshower detectors, an electromagnetic calorimeter and a hadronic calorimeter. Muons are identified by a system composed of alternating layers of iron and multiwire proportional chambers [19].

3 Event simulation

For the event simulation, pp collisions are generated using PYTHIA 6.4 [20] with a specific LHCb configuration [21] using CTEQ6L [22] parton density functions. Decays of hadronic particles are described by EVTGEN [23], in which final-state radiation is generated using PHOTOS [24]. The interaction of the generated particles with the detector and its response are implemented using the GEANT4 toolkit [25,26] as described in Ref. [27].

To simulate a signal event, a SM-like scalar Higgs boson with a mass of 120 GeV/c^2 is generated with PYTHIA through the gluon–gluon fusion mechanism, and is forced to decay into two spin-zero π_v particles, each of which decays to $b\bar{b}$. Assuming the decay occurs via a vector or axial-vector coupling, the $b\bar{b}$ final state is preferred to light quarks, due to helicity conservation [6–8]. The average track multiplicity of the π_v decay, including tracks from secondary b and c decays, varies from about 15 for a π_v mass of 25 GeV/c^2 to about 20 for larger masses. Simulated events are retained if at least four charged tracks from the decay of the generated π_v particles are within the LHCb acceptance, which corresponds to about 30 % of the cases. For π_v particles within the acceptance on average about ten tracks can be reconstructed.

Simulated samples with π_v lifetimes of 10 ps and 100 ps and π_v masses of 25, 35, 43 and 50 GeV/c^2 are generated; other π_v lifetimes are studied by reweighting these samples. Two additional samples are generated in which π_v particles with a lifetime of 10 ps and a mass of 35 GeV/c^2 decay to either $c\bar{c}$ or $s\bar{s}$ quark pairs.

4 Event selection and signal extraction

The selection of candidates starts with the LHCb trigger [28], which consists of a hardware stage, based on information from the calorimeter and muon systems, followed by a software stage, which applies a full event reconstruction. The

hardware trigger (L0) requires a single high-p_T hadron, electron, muon or photon signature. The thresholds range from $p_T > 1.48$ GeV/c for muons, to transverse energy larger than 3.5 GeV for hadrons. The total L0 efficiency, dominated by the hadron trigger selection, depends on the mass and final state of the π_v particle and is typically 20 %, including the detector acceptance.

The software trigger is divided into two stages and consists of algorithms that run a simplified version of the offline track reconstruction, which allows identification of displaced tracks and vertices. For this analysis the primary signature in the first software stage (HLT1) is a single high-quality displaced track with high p_T. The efficiency of HLT1 relative to L0 accepted events is typically 60 %. However, this efficiency reduces rapidly for vertices that are displaced by more than about 5 mm from the beamline due to limitations in the track reconstruction in the vertex detector.

In the final trigger stage (HLT2) two different signatures are exploited. The first of these relies on the generic reconstruction of a displaced vertex, using an algorithm similar to that used for the primary vertex (PV) reconstruction [29]. Secondary vertices are distinguished from PVs using the distance to the interaction region in the transverse plane (R_{xy}). To eliminate contributions from interactions with material, a so-called 'material veto' removes vertices in a region defined as an envelope around the detector material [30]. Events are selected when they have a displaced vertex with at least four tracks, a sum of the scalar p_T of all tracks that is larger than 3 GeV/c, a distance R_{xy} larger than 0.4 mm and an invariant mass of the particles associated with this vertex m_{vtx} above 4.5 GeV/c^2. To further refine the selection, vertices are required to have either $R_{xy} > 2$ mm or $m_{vtx} > 10$ GeV/c^2.

The second HLT2 signature is designed to identify two-, three- and four-body exclusive b-hadron decays [31]. A multivariate algorithm is used for the identification of secondary vertices consistent with the decay of a b hadron. The combined efficiency of the two HLT2 selections relative to events accepted by L0 and HLT1 is about 60 %.

The offline candidate reconstruction starts from a generic secondary vertex search, similar to that applied in the trigger, but using tracks from the offline reconstruction as input. At this stage at least six tracks per vertex are required and the sum of the scalar p_T of all tracks must be above 3 GeV/c. The vertex is required to have either $R_{xy} > 0.4$ mm and $m_{vtx} > 9.7$ GeV/c^2, or $R_{xy} > 2.5$ mm and $m_{vtx} > 8.5$ GeV/c^2, or $R_{xy} > 4$ mm and $m_{vtx} > 6.5$ GeV/c^2.

The vertex reconstruction is followed by a jet reconstruction procedure. Inputs to the jet clustering are obtained using a particle flow approach [32] that selects charged particles, neutral calorimeter deposits and a small contribution from K_s^0 and Λ^0 decays. To reduce contamination from particles that do not originate from the displaced vertex, only charged particles that have a smaller distance of closest approach rel-

ative to the displaced vertex than to any PV in the event are retained. Furthermore, the distance to the displaced vertex is required to be less than 2 mm, which also allows tracks from displaced b and c vertices in the $\pi_v \rightarrow b\bar{b}$ decay chain to be accepted.

The jet clustering uses the anti-k_T algorithm [33] with a cone size of 0.7. Only jets with a p_T above 5 GeV/c are used. Additional requirements are made to enhance the fraction of well-reconstructed hadronic jets: first, the charged particle with the largest p_T in the jet must have a p_T above 0.9 GeV/c, yet carry no more than 70 % of the p_T of the jet. Second, to remove jets whose energy is dominated by neutral particles, which cannot be unambiguously associated with a vertex, at least 10 % of the p_T of the jet must be carried by charged particles.

The di-jet invariant mass is computed from the reconstructed four-momenta of the two jets. Correction factors to the jet energy are determined from the simulation and parameterised as a function of the number of reconstructed PVs in the event, to account for effects due to multiple interactions and the underlying event [32].

Two further requirements are made to enhance signal purity. First, a corrected mass is computed as

$$m_{\text{corr}} = \sqrt{m^2 + (p \sin\theta)^2} + p \sin\theta, \tag{1}$$

where m is the di-jet invariant mass and θ is the pointing angle between the di-jet momentum vector $\mathbf{p}$ and its displacement vector $\mathbf{d} = \mathbf{x}_{\text{DV}} - \mathbf{x}_{\text{PV}}$, where $\mathbf{x}_{\text{DV}}$ is the position of the displaced vertex and $\mathbf{x}_{\text{PV}}$ the position of the PV. To select candidates pointing back to a PV, only events with $m/m_{\text{corr}} > 0.7$ are retained. A requirement on this ratio is preferred over a requirement on the pointing angle itself, since its efficiency depends less strongly on the boost and the mass of the candidate.

Second, a requirement is made on the distance $\Delta R = \sqrt{\Delta\phi^2 + \Delta\eta^2}$ between the two jets, where ϕ is the azimuthal angle and η the pseudorapidity. A background consisting of back-to-back jet candidates, for example di-jet $b\bar{b}$-events, appears mainly at large values of reconstructed mass, and is characterised by a large difference between the jets in both ϕ and η. Only candidates with $\Delta R < 2.2$ are accepted.

Finally, in order to facilitate a reliable estimate of the trigger efficiency, only candidates triggered by particles belonging to one of the jets are kept. Table 1 shows the efficiency to select a π_v particle, for an illustrative mass of 35 GeV/c^2 and lifetime of 10 ps, together with the yield in the data after the most important selection steps. The total efficiency for other masses and lifetimes, as well as for the decays to light quark jets, is shown in Table 2. The efficiencies listed in Tables 1 and 2 represent the number of selected candidates divided by the number of generated events. As the selection efficiencies for the two π_v particles in an event are practically

Table 1 Average number of selected candidates per event (efficiency) in % for the main stages of the offline selection for simulated $H^0 \rightarrow \pi_v\pi_v$ events with $\pi_v \rightarrow b\bar{b}$, $m_{H^0} = 120$ GeV/c^2, $m_{\pi_v} = 35$ GeV/c^2 and $\tau_{\pi_v} = 10$ ps. The pre-selection consists of the acceptance, trigger and offline vertex reconstruction. It represents the first stage in which the candidate yield on the total data sample, shown in the right column, can be counted. The reported uncertainty on the efficiency is only the statistical uncertainty from the finite sample size

Selection step	Signal efficiency	Yield in data
Pre-selection	2.125 ± 0.018	2,555,377
Jet reconstruction	1.207 ± 0.014	117,054
m/m_{corr} and ΔR	0.873 ± 0.012	58,163
Trigger on candidate	0.778 ± 0.012	29,921

Table 2 Average number of selected candidates per event (efficiency) in % for different π_v masses, lifetimes and decay modes. The reported uncertainty is only the statistical uncertainty from the finite sample size. No simulated samples were generated for the 100 ps decay to light quarks

Decay	m_{π_v} [GeV/c^2]	Signal efficiency	
		$\tau_{\pi_v} = 10$ ps	$\tau_{\pi_v} = 100$ ps
$\pi_v \rightarrow b\bar{b}$	25	0.373 ± 0.008	0.0805 ± 0.0019
	35	0.778 ± 0.012	0.181 ± 0.005
	43	0.743 ± 0.011	0.183 ± 0.003
	50	0.573 ± 0.015	0.154 ± 0.004
$\pi_v \rightarrow c\bar{c}$	35	2.18 ± 0.05	–
$\pi_v \rightarrow s\bar{s}$	35	2.06 ± 0.04	–

independent, the fraction of selected events with more than one candidate is less than a few percent in simulated signal. In data no events with more than one π_v candidate are found.

Figure 1 shows the mass and p_T distributions for selected di-jet candidates in data and in simulated signal events, assuming a π_v particle with a mass of 25, 35 or 50 GeV/c^2. The turn-on at low values in the mass distribution of events observed in data (Fig. 1a) is caused by the minimum p_T requirement on the jets. The rest of the distribution falls off exponentially. The p_T distribution shown in Fig. 1b illustrates that long-lived particles with a higher mass have lower p_T as there is less momentum available in the Higgs decay. This affects the selection efficiency since for a given decay time the transverse decay length is proportional to p_T.

Studies on simulated events have shown that both the shape and the normalisation of the mass distribution in data are compatible with the expected background from $b\bar{b}$ production. It is not possible to generate sufficiently large samples of $b\bar{b}$ events to use these for a quantitative estimate of the background after the final selection. Therefore, the signal yield is extracted by a fit to the invariant mass distribution assuming a smooth shape for the background, as discussed in Sect. 6.
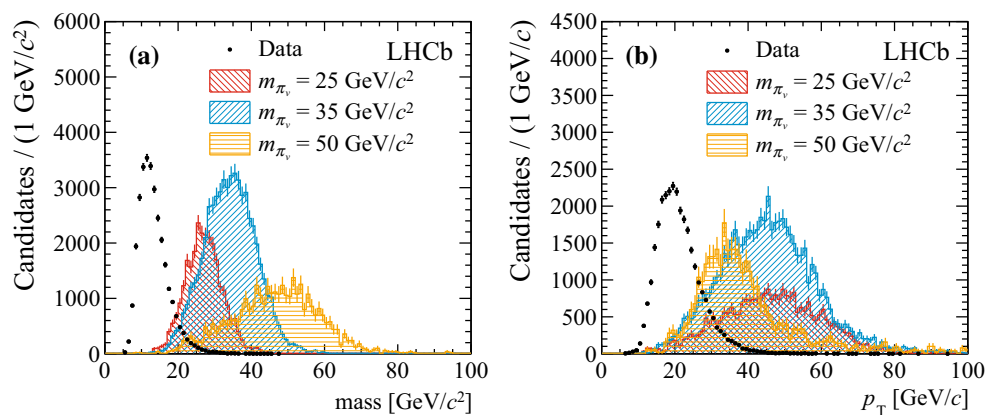
Fig. 1 Invariant mass (**a**) and p_T distribution (**b**) for di-jet candidates in data and in hidden valley models with 25, 35 and 50 GeV/c^2 π_v masses and 10 ps lifetime. For visibility, the simulated signal is scaled to 0.62 fb^{-1} assuming a Higgs cross-section of 10 nb and branching fractions of 100 % for $\mathcal{B}(H \to \pi_v \pi_v)$ and $\mathcal{B}(\pi_v \to b\bar{b})$
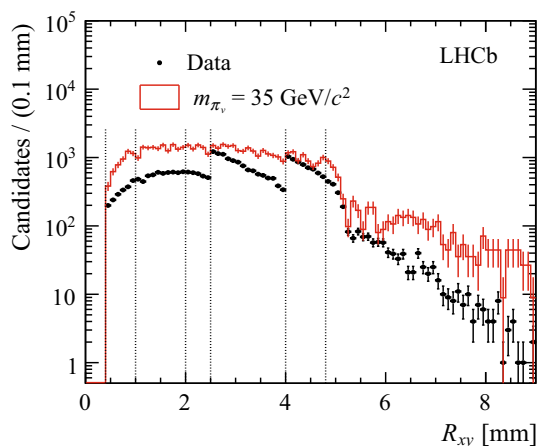

Fig. 2 Distribution of the distance of the displaced vertex to the interaction region in the transverse plane for data and for a hidden valley model with $m_{\pi_v} = 35$ GeV/c^2 and $\tau_{\pi_v} = 10$ ps after the full selection. For visibility, the simulated signal is scaled to 0.62 fb^{-1} assuming a Higgs cross-section of 10 nb and branching fractions of 100 % for $\mathcal{B}(H \to \pi_v \pi_v)$ and $\mathcal{B}(\pi_v \to b\bar{b})$. The boundaries of the intervals used in the fit are indicated by the dotted lines. The generated R_{xy} distribution is approximately exponential with an average of about 2 mm

Since the background yield, the shape of the background invariant mass distribution and the selection efficiency strongly depend on the radial displacement R_{xy}, limits are extracted from a simultaneous maximum likelihood fit to the di-jet invariant mass distribution in five bins of R_{xy}. The intervals are chosen in the most sensitive region, between 0.4 and 4.8 mm. The events at larger radii are not used as they contribute only marginally to the sensitivity. Figure 2 shows the distribution of R_{xy} of selected displaced vertices for data and simulated signal events, together with the bin boundaries. The effect of the reduction in efficiency at large radii due to the material veto and the HLT1 trigger is visible, as is the effect of requirements on R_{xy} in the trigger. The trigger effects are more pronounced in data than in simulated

signal, because signal events are less affected by cuts on the vertex invariant mass.

The background di-jet invariant mass distribution is characterised by an exponential falloff, with a low-mass threshold determined mostly by the minimum p_T requirement of the jets. It is modelled by a single-sided exponential function convoluted with a bifurcated Gaussian function. The parameters of the background model are fitted to data, independently in each R_{xy} bin. The signal is modelled by a bifurcated Gaussian function, whose parameters are determined from simulated events in bins of R_{xy}. The effect of the uncertainty on the jet-energy scale is included by a scale parameter for the mass, which is common to all bins and constrained using a sample of $Z +$ jet events, as explained in Sect. 5. Additional nuisance parameters are added to account for the finite statistics of the simulated samples and the systematic uncertainties on the signal efficiency and the luminosity. The fit model is implemented using the ROOFIT [34] package. Figure 3 shows the fit result in the five radial bins for a signal model with $m_{\pi_v} = 35$ GeV/c^2 and $\tau_{\pi_v} = 10$ ps.

5 Systematic uncertainties

Several sources of systematic uncertainties have been considered. The uncertainties depend on the π_v mass and are summarised in Table 3. The uncertainty on the vertex finding efficiency is assessed by comparing the efficiency of the vertexing algorithm on a sample of $B^0 \to j/\psi K^{*0}$ with $K^{*0} \to K^+\pi^-$ events in data and simulation as a function of R_{xy}. The efficiency difference is about 7.5 % at large R_{xy}, which is taken as an estimate of the uncertainty on the vertex finding algorithm efficiency. Since the B^0 vertices have only four tracks, and the π_v decays studied in this paper have typically more tracks, this is considered a conservative estimate. The uncertainty on the track
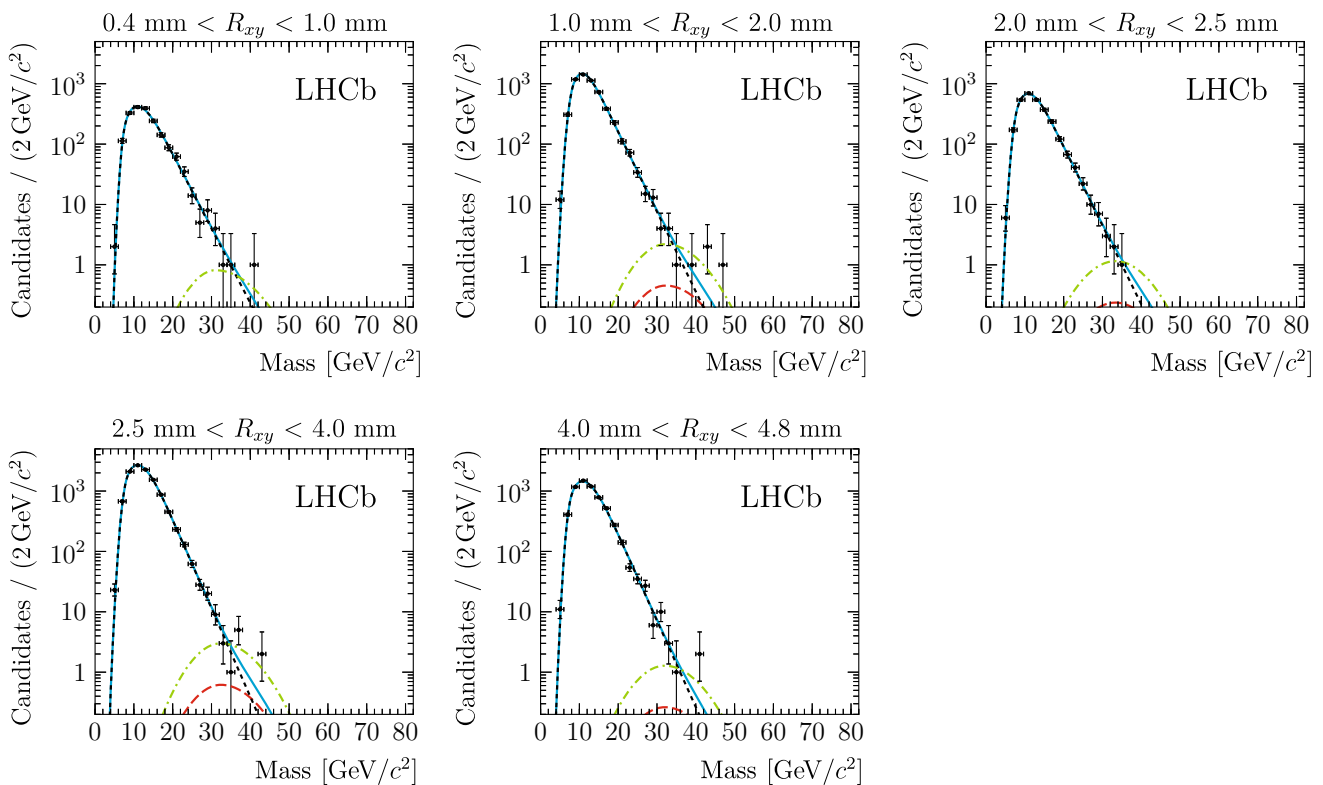
Fig. 3 Di-jet invariant mass distributions for each of the five R_{xy} bins, superimposed with the fits for a hidden valley model with $m_{\pi_v} = 35\,\text{GeV}/c^2$ and $\tau_{\pi_v} = 10\,\text{ps}$. The *blue line* indicates the result of the total fit to the data. The *black short-dashed line* is the background-only contribution, and the *red long-dashed line* is the fitted signal contribution. For illustration, the *green dash-dotted line* shows the signal scaled to a cross-section of 17 pb, which corresponds to the SM Higgs production cross-section at 7 TeV [35]

finding efficiency for prompt tracks in LHCb is 1.4 % per track, with a small dependence on track kinematics [36]. The uncertainty for displaced tracks was evaluated in the context of a recent LHCb measurement of b-hadron lifetimes [37] and extrapolated to larger R_{xy}, leading to a per-track uncertainty of 2 %. Due to requirements on the minimal number of tracks in the vertex, this translates into an uncertainty on the vertex finding efficiency, which is estimated to be 2 % for signal events. Adding in quadrature the track efficiency and the vertex finding algorithm efficiency uncertainties leads to a total uncertainty of 7.9 % on the vertex reconstruction. The selection on the vertex sum-p_{T} and mass is affected by the track finding efficiency as well. Propagating the per-track uncertainty leads to an uncertainty on the vertex selection efficiency of up to 2.9 %, depending on the π_v mass.

The uncertainties related to the jet selection are determined by comparing jets in data and simulation on a sample of $Z+$jet events, analogously to a recent LHCb measurement of $Z+$jet production [32]. The Z candidate is reconstructed in the $\mu^+\mu^-$ final state from two oppositely charged tracks, identified as muons, that form a good vertex and have an invariant mass in the range 60–120 GeV/c^2. Jets are recon-

Table 3 Systematic uncertainties on the selection efficiency and luminosity for simulated hidden valley events with a lifetime of 10 ps and various π_v masses

Source	Relative uncertainty (%)			
π_v Mass [GeV/c^2]	25	35	43	50
Vertex reconstruction	7.9	7.9	7.9	7.9
Vertex scalar-p_{T} and mass	2.9	2.3	2.0	1.7
Jet reconstruction	1.3	0.6	0.4	0.3
Jet identification	2.9	3.0	3.2	3.2
Jet pointing	4.6	2.9	2.6	2.0
L0 trigger	4.6	4.5	4.5	4.4
HLT1 trigger	4.1	4.0	4.0	4.3
HLT2 trigger	5.9	5.9	6.1	6.3
Luminosity	1.7	1.7	1.7	1.7
Total	13.3	12.7	12.6	12.6

structed using the same selection of input particles as in the reconstruction of jets for long-lived particles, except that the origin vertex is in this case the PV consistent with the Z vertex. The differences between data and simulation in the $Z+$jet sample are parameterised as function of the jet p_{T}

and subsequently propagated to the simulated hidden valley signal samples.

The uncertainty on the jet energy scale is derived from the ratio of transverse momenta of the jet and the Z, which are expected to have a back-to-back topology, and correlated transverse momenta. Data and simulation agree within about 2 %, resulting in an uncertainty on the di-jet invariant mass scale of 4 %. This uncertainty on the signal shape is taken into account in the fitting procedure. The uncertainty on the jet-energy scale also affects the jet reconstruction efficiency due to the requirement on the minimum jet p_T. It leads to an uncertainty on the efficiency between 0.3 and 1.3 %, depending on the assumed π_v particle mass. The uncertainty on the hadronic jet identification requirements are assessed using the $Z + $ jet sample as well and amount to about 3 %.

The resolutions on the pointing angle θ and on ΔR are dominated by the resolution on the direction of the π_v candidate, which in turn is determined by the jet angular resolution. The latter is estimated from the difference between data and simulation in the resolution of the azimuthal angle between the jet and the Z. Due to the limited statistics in the $Z + $ jet sample a relatively large uncertainty between 2.0 and 4.6 % is obtained, depending on the π_v mass.

The trigger selection efficiency on signal is determined from the simulation. The trigger efficiencies in data and simulation are compared using a sample of generic $B \rightarrow J/\psi X$ events that contain an offline reconstructed displaced vertex, but are triggered independently of the displaced vertex trigger lines. The integrated efficiency difference for the trigger stages L0, HLT1 and HLT2 amounts to systematic uncertainties of at most 4.6, 4.3 and 6.3 % respectively. This is a conservative estimate since the trigger efficiencies for the sample of displaced J/ψ vertices are smaller than the efficiencies for the signal, which consists of heavier, more displaced objects with a larger number of tracks. Finally, the uncertainty on the luminosity at the LHCb interaction point is 1.7 % [38].

Several alternatives have been considered for the background mass model, in particular with an additional expo-

nential component, or a component that is independent of the mass. With these models the estimated background yield at higher mass is larger than with the nominal background model, leading to tighter limits on the signal. As the nominal model gives the most conservative limit, no additional systematic uncertainty is assigned.

6 Results

The fit procedure is performed for a π_v mass of 25, 35, 43 and 50 GeV/c^2 and for several values of the lifetime in between 1 and 200 ps. No significant signal is observed for any combination of π_v mass and lifetime. Upper limits are extracted using the CL$_s$ method [39] with a frequentist treatment of the nuisance parameters described above, as implemented in the ROOSTATS [40] package.

Limits are set on the Higgs production cross-section multiplied by the branching fraction into long-lived particles $\sigma(H) \times \mathcal{B}(H \rightarrow \pi_v \pi_v)$. In the simulation it is assumed that both π_v particles decay to the same final state. If the decay width of the π_v particle is dominated by final states other than $q\bar{q}$, the limits scale as $1/(\mathcal{B}_{q\bar{q}}(2 - \mathcal{B}_{q\bar{q}}))$ where $\mathcal{B}_{q\bar{q}}$ is the $\pi_v \rightarrow q\bar{q}$ branching fraction. The obtained 95 % CL upper limits on $\sigma(H) \times \mathcal{B}(H \rightarrow \pi_v \pi_v)$, under the assumption of a 100 % branching fraction to $b\bar{b}$, are shown in Table 4 and in Fig. 4. As the background decreases with the observed di-jet invariant mass, the limits become stronger with increasing π_v mass. The sensitivity has an optimal value at a lifetime of about 5 ps.

Additional limits are set on models with a π_v particle decaying to $c\bar{c}$ and to $s\bar{s}$. The limits for π_v decay to $u\bar{u}$ and $d\bar{d}$ are expected to be the same as for $s\bar{s}$. The light quark decays result in a higher displaced vertex track multiplicity, and lighter jets, leading to a higher selection efficiency. Consequently, the limits for decays to light quark jets are more stringent than those for decays to b-quark jets.

Table 4 Observed 95 % CL cross-section upper limits on $\sigma(H) \times \mathcal{B}(H \rightarrow \pi_v \pi_v)$ (in pb) on a hidden valley [6–8] model for various π_v masses and lifetimes. Both π_v particles are assumed to decay into $b\bar{b}$, unless specified otherwise

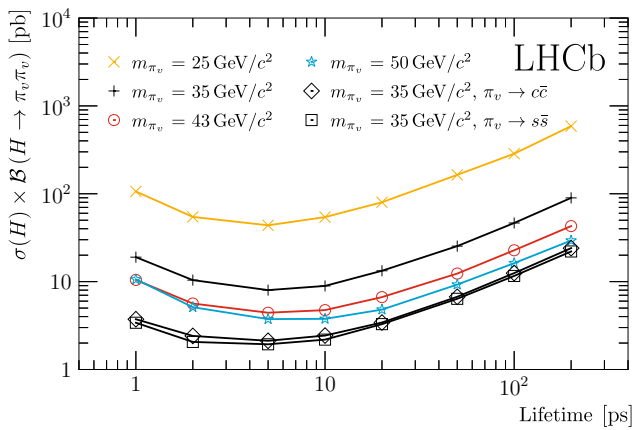| π_v Mass [GeV/c^2]	π_v Lifetime [ps]							
	1	2	5	10	20	50	100	200
25	106.3	54.6	43.8	54.2	80.0	164.1	285.7	588.5
35	19.0	10.4	8.0	8.9	13.3	25.4	46.5	89.8
43	10.5	5.6	4.4	4.7	6.7	12.4	22.7	42.8
50	10.6	5.1	3.7	3.8	4.8	9.3	16.2	29.3
35 ($\pi_v \rightarrow c\bar{c}$)	3.7	2.4	2.1	2.4	3.4	6.7	12.5	24.1
35 ($\pi_v \rightarrow s\bar{s}$)	3.4	2.1	1.9	2.2	3.3	6.4	11.6	22.0

Fig. 4 Observed 95 % CL cross-section upper limits on a hidden valley model [6–8] for various π_v masses, as a function of π_v lifetime. Both π_v particles are assumed to decay into $b\bar{b}$, unless specified otherwise

7 Conclusion

A search has been presented for massive, long-lived particles in a sample of pp collisions at $\sqrt{s} = 7$ TeV, corresponding to an integrated luminosity of 0.62 fb^{-1}, collected by the LHCb experiment. The long-lived spin-zero particles are assumed to be pair-produced in the decay of a 120 GeV/c^2 SM Higgs, and to decay to two hadronic jets. They appear for instance as π_v particles in hidden valley models. A single π_v particle is identified by a displaced vertex and two associated jets. No significant signal for π_v particles with a mass between 25 and 50 GeV/c^2 and a lifetime between 1 and 200 ps is observed. Assuming a 100% branching fraction to b-quark jets, the 95 % CL upper limits on the production cross-section $\sigma(H) \times \mathcal{B}(H \to \pi_v\pi_v)$ are in the range 4–600 pb.

The results cover a region in mass and lifetime that so far has been unexplored at the LHC. The obtained upper limits are more restrictive than results from the Tevatron experiments in the same mass and lifetime region. The best sensitivity is obtained for π_v particles with a lifetime of about 5 ps and a mass above approximately 40 GeV/c^2. The SM Higgs cross-section at 7 TeV is about 17 pb [35]. The measurements in the most sensitive region exclude branching fractions of greater than 25 % for a SM Higgs boson to pair produce π_v particles that decay to two hadronic jets.

References

1. L.M. Carpenter, D.E. Kaplan, E.-J. Rhee, Six-quark decays of the Higgs boson in supersymmetry with R-parity violation. Phys. Rev. Lett. **99**, 211801 (2007). arXiv:hep-ph/0607204
2. J.M. Butterworth, J.R. Ellis, A.R. Raklev, G.P. Salam, Discovering baryon-number violating neutralino decays at the LHC. Phys. Rev. Lett. **103**, 241803 (2009). arXiv:0906.0728
3. D.E. Kaplan, K. Rehermann, Proposal for Higgs and superpartner searches at the LHCb experiment. JHEP **10**, 056 (2007). arXiv:0705.3426
4. F. de Campos, O.J.P. Eboli, M.B. Magro, D. Restrepo, Searching supersymmetry at the LHCb with displaced vertices. Phys. Rev. D **79**, 055008 (2009). arXiv:0809.0007
5. F. de Campos, M.B. Magro, Displaced vertices in GMSB models at LHC. arXiv:1306.5773
6. M.J. Strassler, K.M. Zurek, Echoes of a hidden valley at hadron colliders. Phys. Lett. B **651**, 374 (2007). arXiv:hep-ph/0604261
7. M.J. Strassler, K.M. Zurek, Discovering the Higgs through highly-displaced vertices. Phys. Lett. B **661**, 263 (2008). arXiv:hep-ph/0605193
8. T. Han, Z. Si, K.M. Zurek, M.J. Strassler, Phenomenology of hidden valleys at hadron colliders. JHEP **07**, 008 (2008). arXiv:0712.2041
9. ATLAS Collaboration, G. Aad et al., Observation of a new particle in the search for the standard model Higgs boson with the ATLAS detector at the LHC. Phys. Lett. B **716**, 1 (2012). arXiv:1207.7214
10. CMS Collaboration, S. Chatrchyan et al., Observation of a new boson at a mass of 125 GeV with the CMS experiment at the LHC. Phys. Lett. B **716**, 30 (2012). arXiv:1207.7235
11. CDF Collaboration, T. Aaltonen et al., Search for heavy metastable particles decaying to jet pairs in $p\bar{p}$ collisions at $\sqrt{s} = 1.96$ TeV. Phys. Rev. D **85**, 012007 (2012). arXiv:1109.3136
12. D0 collaboration, V. M. Abazov et al., Search for resonant pair production of neutral long-Lived particles decaying to $b\bar{b}$ in $p\bar{p}$ collisions at $\sqrt{s} = 1.96$TeV. Phys. Rev. Lett. **103**, 071801 (2009). arXiv:0906.1787
13. ATLAS Collaboration, G. Aad et al., Search for a light Higgs boson decaying to long-lived weakly-interacting particles in proton–proton collisions at $\sqrt{s} = 7$ TeV with the ATLAS detector. Phys. Rev. Lett. **108**, 251801 (2012). arXiv:1203.1303
14. CMS Collaboration, V. Khachatryan et al., Search for long-lived neutral particles decaying to quark–antiquark pairs in proton–proton collisions at $\sqrt{s} = 8$ TeV. Phys. Rev. D **91**(1), 012007 (2015). doi:10.1103/PhysRevD.91.012007. arXiv:1411.6530 [hep-ex]

15. LHCb Collaboration, A.A. Alves Jr. et al., The LHCb detector at the LHC. JINST **3**, S08005 (2008)
16. R. Aaij et al., Performance of the LHCb vertex locator. JINST **9**, 09007 (2014). arXiv:1405.7808
17. R. Arink et al., Performance of the LHCb outer tracker. JINST **9**, P01002 (2014). arXiv:1311.3893
18. M. Adinolfi et al., Performance of the LHCb RICH detector at the LHC. Eur. Phys. J. C **73**, 2431 (2013). arXiv:1211.6759
19. A.A. Alves Jr et al., Performance of the LHCb muon system. JINST **8**, P02022 (2013). arXiv:1211.1346
20. T. Sjöstrand, S. Mrenna, P. Skands, PYTHIA 6.4 physics and manual. JHEP **05**, 026 (2006). arXiv:hep-ph/0603175
21. I. Belyaev et al., Handling of the generation of primary events in Gauss, the LHCb simulation framework. in *Nuclear Science Symposium Conference Record (NSS/MIC) IEEE* (2010), p. 1155
22. J. Pumplin et al., New generation of parton distributions with uncertainties from global QCD analysis. JHEP **07**, 012 (2002). arXiv:hep-ph/0201195
23. D.J. Lange, The EvtGen particle decay simulation package. Nucl. Instrum. Methods A **462**, 152 (2001)
24. P. Golonka, Z. Was, PHOTOS Monte Carlo: a precision tool for QED corrections in Z and W decays. Eur. Phys. J. C **45**, 97 (2006). arXiv:hep-ph/0506026
25. Geant4 Collaboration, J. Allison et al., Geant4 developments and applications. IEEE Trans. Nucl. Sci. **53**, 270 (2006)
26. Geant4 Collaboration, S. Agostinelli et al., Geant4: a simulation toolkit. Nucl. Instrum. Methods A **506**, 250 (2003)
27. M. Clemencic et al., The LHCb simulation application, Gauss: design, evolution and experience. J. Phys. Conf. Ser. **331**, 032023 (2011)
28. R. Aaij et al., The LHCb trigger and its performance in 2011. JINST **8**, P04022 (2013). arXiv:1211.3055
29. M. Kucharczyk, P. Morawski, M. Witek, Primary vertex reconstruction at LHCb. LHCb-PUB-2014-044
30. LHCb Collaboration, R. Aaij et al., Search for the rare decay $K_S^0 \to \mu^+\mu^-$. JHEP **01**, 090 (2013). doi:10.1007/JHEP01(2013)090. arXiv:1209.4029 [hep-ex]
31. V.V. Gligorov, M. Williams, Efficient, reliable and fast high-level triggering using a bonsai boosted decision tree. JINST **8**, P02013 (2013). arXiv:1210.6861
32. LHCb Collaboration, R. Aaij et al., Study of forward Z+jet production in pp collisions at $\sqrt{s}$ = 7 TeV. JHEP **01**, 033 (2014). doi:10.1007/JHEP01(2014)033. arXiv:1310.8197 [hep-ex]
33. M. Cacciari, G.P. Salam, G. Soyez, The anti-k_T jet clustering algorithm. JHEP **04**, 063 (2008). arXiv:0802.1189
34. W. Verkerke, D.P. Kirkby, The RooFit toolkit for data modeling. eConf **C0303241**, MOLT007 (2003). arXiv:physics/0306116
35. LHC Higgs Cross Section Working Group, S. Heinemeyer et al., Handbook of LHC Higgs cross sections: 3. Higgs properties. (2013). doi:10.5170/CERN-2013-004. arXiv:1307.1347 [hep-ex]
36. LHCb Collaboration, R. Aaij et al., Measurement of the track reconstruction efficiency at LHCb. JINST **10**, P02007 (2015). doi:10.1088/1748-0221/10/02/P02007. arXiv:1408.1251 [hep-ex]
37. LHCb Collaboration, R. Aaij et al., Measurements of the B^+, B^0, B_s^0 meson and Λ_b^0 baryon lifetimes. JHEP **04**, 114 (2014). arXiv:1402.2554
38. LHCb Collaboration, R. Aaij et al., Precision luminosity measurements at LHCb. JINST **9**, P12005 (2014). arXiv:1410.0149
39. A.L. Read, Presentation of search results: the CL(s) technique. J. Phys. G **28**, 2693 (2002)
40. L. Moneta et al., The RooStats Project. PoS **ACAT2010**, 057 (2010). arXiv:1009.1003

LHCb Collaboration

R. Aaij[41], B. Adeva[37], M. Adinolfi[46], A. Affolder[52], Z. Ajaltouni[5], S. Akar[6], J. Albrecht[9], F. Alessio[38], M. Alexander[51], S. Ali[41], G. Alkhazov[30], P. Alvarez Cartelle[37], A. A. AlvesJr[25,38], S. Amato[2], S. Amerio[22], Y. Amhis[7], L. An[3], L. Anderlini[17,g], J. Anderson[40], R. Andreassen[57], M. Andreotti[16,f], J. E. Andrews[58], R. B. Appleby[54], O. Aquines Gutierrez[10], F. Archilli[38], A. Artamonov[35], M. Artuso[59], E. Aslanides[6], G. Auriemma[25,n], M. Baalouch[5], S. Bachmann[11], J. J. Back[48], A. Badalov[36], C. Baesso[60], W. Baldini[16], R. J. Barlow[54], C. Barschel[38], S. Barsuk[7], W. Barter[47], V. Batozskaya[28], V. Battista[39], A. Bay[39], L. Beaucourt[4], J. Beddow[51], F. Bedeschi[23], I. Bediaga[1], S. Belogurov[31], K. Belous[35], I. Belyaev[31], E. Ben-Haim[8], G. Bencivenni[18], S. Benson[38], J. Benton[46], A. Berezhnoy[32], R. Bernet[40], A. Bertolin[22], M.-O. Bettler[47], M. van Beuzekom[41], A. Bien[11], S. Bifani[45], T. Bird[54], A. Bizzeti[17,i], P. M. Bjørnstad[54], T. Blake[48], F. Blanc[39], J. Blouw[10], S. Blusk[59], V. Bocci[25], A. Bondar[34], N. Bondar[30,38], W. Bonivento[15], S. Borghi[54], A. Borgia[59], M. Borsato[7], T. J. V. Bowcock[52], E. Bowen[40], C. Bozzi[16], D. Brett[54], M. Britsch[10], T. Britton[59], J. Brodzicka[54], N. H. Brook[46], A. Bursche[40], J. Buytaert[38], S. Cadeddu[15], R. Calabrese[16,f], M. Calvi[20,k], M. Calvo Gomez[36,p], P. Campana[18], D. Campora Perez[38], L. Capriotti[54], A. Carbone[14,d], G. Carboni[24,l], R. Cardinale[19,38,j], A. Cardini[15], L. Carson[50], K. Carvalho Akiba[2,38], RCM Casanova Mohr[36], G. Casse[52], L. Cassina[20,k], L. Castillo Garcia[38], M. Cattaneo[38], Ch. Cauet[9], R. Cenci[23,t], M. Charles[8], Ph. Charpentier[38], M. Chefdeville[4], S. Chen[54], S.-F. Cheung[55], N. Chiapolini[40], M. Chrzaszcz[26,40], X. Cid Vidal[38], G. Ciezarek[41], P. E. L. Clarke[50], M. Clemencic[38], H. V. Cliff[47], J. Closier[38], V. Coco[38], J. Cogan[6], E. Cogneras[5], V. Cogoni[15,e], L. Cojocariu[29], G. Collazuol[22], P. Collins[38], A. Comerma-Montells[11], A. Contu[15,38], A. Cook[46], M. Coombes[46], S. Coquereau[8], G. Corti[38], M. Corvo[16,f], I. Counts[56], B. Couturier[38], G. A. Cowan[50], D. C. Craik[48], A.C. Crocombe[48], M. Cruz Torres[60], S. Cunliffe[53], R. Currie[53], C. D'Ambrosio[38], J. Dalseno[46], P. David[8], P. N. Y. David[41], A. Davis[57], K. De Bruyn[41], S. De Capua[54], M. De Cian[11], J. M. De Miranda[1], L. De Paula[2], W. De Silva[57], P. De Simone[18], C.-T. Dean[51], D. Decamp[4], M. Deckenhoff[9], L. Del Buono[8], N. Déléage[4], D. Derkach[55], O. Deschamps[5], F. Dettori[38], B. Dey[40], A. Di Canto[38], A Di Domenico[25], H. Dijkstra[38], S. Donleavy[52], F. Dordei[11], M. Dorigo[39], A. Dosil Suárez[37], D. Dossett[48], A. Dovbnya[43], K. Dreimanis[52], G. Dujany[54], F. Dupertuis[39], P. Durante[38], R. Dzhelyadin[35], A. Dziurda[26], A. Dzyuba[30], S. Easo[38,49],

U. Egede[53], V. Egorychev[31], S. Eidelman[34], S. Eisenhardt[50], U. Eitschberger[9], R. Ekelhof[9], L. Eklund[51], I. El Rifai[5], Ch. Elsasser[40], S. Ely[59], S. Esen[11], H.-M. Evans[47], T. Evans[55], A. Falabella[14], C. Färber[11], C. Farinelli[41], N. Farley[45], S. Farry[52], R. Fay[52], D. Ferguson[50], V. Fernandez Albor[37], F. Ferreira Rodrigues[1], M. Ferro-Luzzi[38], S. Filippov[33], M. Fiore[16,f], M. Fiorini[16,f], M. Firlej[27], C. Fitzpatrick[39], T. Fiutowski[27], P. Fol[53], M. Fontana[10], F. Fontanelli[19,j], R. Forty[38], O. Francisco[2], M. Frank[38], C. Frei[38], M. Frosini[17], J. Fu[21,38], E. Furfaro[24,l], A. Gallas Torreira[37], D. Galli[14,d], S. Gallorini[22,38], S. Gambetta[19,j], M. Gandelman[2], P. Gandini[59], Y. Gao[3], J. García Pardiñas[37], J. Garofoli[59], J. Garra Tico[47], L. Garrido[36], D. Gascon[36], C. Gaspar[38], U. Gastaldi[16], R. Gauld[55], L. Gavardi[9], G. Gazzoni[5], A. Geraci[21,v], E. Gersabeck[11], M. Gersabeck[54], T. Gershon[48], Ph. Ghez[4], A. Gianelle[22], S. Gianì[39], V. Gibson[47], L. Giubega[29], V. V. Gligorov[38], C. Göbel[60], D. Golubkov[31], A. Golutvin[31,38,53], A. Gomes[1,a], C. Gotti[20,k], M. Grabalosa Gándara[5], R. Graciani Diaz[36], L. A. Granado Cardoso[38], E. Graugés[36], E. Graverini[40], G. Graziani[17], A. Grecu[29], E. Greening[55], S. Gregson[47], P. Griffith[45], L. Grillo[11], O. Grünberg[63], B. Gui[59], E. Gushchin[33], Yu. Guz[35,38], T. Gys[38], C. Hadjivasiliou[59], G. Haefeli[39], C. Haen[38], S. C. Haines[47], S. Hall[53], B. Hamilton[58], T. Hampson[46], X. Han[11], S. Hansmann-Menzemer[11], N. Harnew[55], S. T. Harnew[46], J. Harrison[54], J. He[38], T. Head[39], V. Heijne[41], K. Hennessy[52], P. Henrard[5], L. Henry[8], J. A. Hernando Morata[37], E. van Herwijnen[38], M. Heß[63], A. Hicheur[2], D. Hill[55], M. Hoballah[5], C. Hombach[54], W. Hulsbergen[41], N. Hussain[55], D. Hutchcroft[52], D. Hynds[51], M. Idzik[27], P. Ilten[56], R. Jacobsson[38], A. Jaeger[11], J. Jalocha[55], E. Jans[41], A. Jawahery[58], F. Jing[3], M. John[55], D. Johnson[38], C. R. Jones[47], C. Joram[38], B. Jost[38], N. Jurik[59], S. Kandybei[43], W. Kanso[6], M. Karacson[38], T. M. Karbach[38], S. Karodia[51], M. Kelsey[59], I. R. Kenyon[45], T. Ketel[42], B. Khanji[20,38,k], C. Khurewathanakul[39], S. Klaver[54], K. Klimaszewski[28], O. Kochebina[7], M. Kolpin[11], I. Komarov[39], R. F. Koopman[42], P. Koppenburg[41,38], M. Korolev[32], L. Kravchuk[33], K. Kreplin[11], M. Kreps[48], G. Krocker[11], P. Krokovny[34], F. Kruse[9], W. Kucewicz[26,o], M. Kucharczyk[20,26,k], V. Kudryavtsev[34], K. Kurek[28], T. Kvaratskheliya[31], V. N. La Thi[39], D. Lacarrere[38], G. Lafferty[54], A. Lai[15], D. Lambert[50], R. W. Lambert[42], G. Lanfranchi[18], C. Langenbruch[48], B. Langhans[38], T. Latham[48], C. Lazzeroni[45], R. Le Gac[6], J. van Leerdam[41], J.-P. Lees[4], R. Lefèvre[5], A. Leflat[32], J. Lefrançois[7], O. Leroy[6], T. Lesiak[26], B. Leverington[11], Y. Li[3], T. Likhomanenko[64], M. Liles[52], R. Lindner[38], C. Linn[38], F. Lionetto[40], B. Liu[15], S. Lohn[38], I. Longstaff[51], J. H. Lopes[2], P. Lowdon[40], D. Lucchesi[22,r], H. Luo[50], A. Lupato[22], E. Luppi[16,f], O. Lupton[55], F. Machefert[7], I. V. Machikhiliyan[31], F. Maciuc[29], O. Maev[30], S. Malde[55], A. Malinin[64], G. Manca[15,e], G. Mancinelli[6], A. Mapelli[38], J. Maratas[5], J.F. Marchand[4], U. Marconi[14], C. Marin Benito[36], P. Marino[23,t], R. Märki[39], J. Marks[11], G. Martellotti[25], M. Martinelli[39], D. Martinez Santos[42], F. Martinez Vidal[65], D. Martins Tostes[2], A. Massafferri[1], R. Matev[38], Z. Mathe[38], C. Matteuzzi[20], A. Mazurov[45], M. McCann[53], J. McCarthy[45], A. McNab[54], R. McNulty[12], B. McSkelly[52], B. Meadows[57], F. Meier[9], M. Meissner[11], M. Merk[41], D. A. Milanes[62], M.-N. Minard[4], N. Moggi[14], J. Molina Rodriguez[60], S. Monteil[5], M. Morandin[22], P. Morawski[27], A. Mordà[6], M. J. Morello[23,t], J. Moron[27], A.-B. Morris[50], R. Mountain[59], F. Muheim[50], K. Müller[40], M. Mussini[14], B. Muster[39], P. Naik[46], T. Nakada[39], R. Nandakumar[49], I. Nasteva[2], M. Needham[50], N. Neri[21], S. Neubert[38], N. Neufeld[38], M. Neuner[11], A. D. Nguyen[39], T. D. Nguyen[39], C. Nguyen-Mau[39,q], M. Nicol[7], V. Niess[5], R. Niet[9], N. Nikitin[32], T. Nikodem[11], A. Novoselov[35], D. P. O'Hanlon[48], A. Oblakowska-Mucha[27], V. Obraztsov[35], S. Ogilvy[51], O. Okhrimenko[44], R. Oldeman[15,e], C. J. G. Onderwater[66], M. Orlandea[29], B. Osorio Rodrigues[1], J. M. Otalora Goicochea[2], A. Otto[38], P. Owen[53], A. Oyanguren[65], B. K. Pal[59], A. Palano[13,c], F. Palombo[21,u], M. Palutan[18], J. Panman[38], A. Papanestis[38,49], M. Pappagallo[51], L. L. Pappalardo[16,f], C. Parkes[54], C. J. Parkinson[9,45], G. Passaleva[17], G. D. Patel[52], M. Patel[53], C. Patrignani[19,j], A. Pearce[54,49], A. Pellegrino[41], G. Penso[25,m], M. Pepe Altarelli[38], S. Perazzini[14,d], P. Perret[5], L. Pescatore[45], E. Pesen[67], K. Petridis[53], A. Petrolini[19,j], E. Picatoste Olloqui[36], B. Pietrzyk[4], T. Pilař[48], D. Pinci[25], A. Pistone[19], S. Playfer[50], M. Plo Casasus[37], F. Polci[8], A. Poluektov[34,48], I. Polyakov[31], E. Polycarpo[2], A. Popov[35], D. Popov[10], B. Popovici[29], C. Potterat[2], E. Price[46], J.D. Price[52], J. Prisciandaro[39], A. Pritchard[52], C. Prouve[46], V. Pugatch[44], A. Puig Navarro[39], G. Punzi[23,s], W. Qian[4], B. Rachwal[26], J. H. Rademacker[46], B. Rakotomiaramanana[39], M. Rama[23], M. S. Rangel[2], I. Raniuk[43], N. Rauschmayr[38], G. Raven[42], F. Redi[53], S. Reichert[54], M. M. Reid[48], A. C. dos Reis[1], S. Ricciardi[49], S. Richards[46], M. Rihl[38], K. Rinnert[52], V. Rives Molina[36], P. Robbe[7], A. B. Rodrigues[1], E. Rodrigues[54], P. Rodriguez Perez[54], S. Roiser[38], V. Romanovsky[35], A. Romero Vidal[37], M. Rotondo[22], J. Rouvinet[39], T. Ruf[38], H. Ruiz[36], P. Ruiz Valls[65], J. J. Saborido Silva[37], N. Sagidova[30], P. Sail[51], B. Saitta[15,e], V. Salustino Guimaraes[2], C. Sanchez Mayordomo[65], B. Sanmartin Sedes[37], R. Santacesaria[25], C. Santamarina Rios[37], E. Santovetti[24,l], A. Sarti[18,m], C. Satriano[25,n], A. Satta[24], D.M. Saunders[46], D. Savrina[31,32], M. Schiller[38], H. Schindler[38], M. Schlupp[9], M. Schmelling[10], B. Schmidt[38], O. Schneider[39], A. Schopper[38], M.-H. Schune[7], R. Schwemmer[38], B. Sciascia[18], A. Sciubba[25,m], A. Semennikov[31], I. Sepp[53], N. Serra[40], J. Serrano[6], L. Sestini[22], P. Seyfert[11], M. Shapkin[35], I. Shapoval[16,43,f], Y. Shcheglov[30], T. Shears[52], L. Shekhtman[34], V. Shevchenko[64], A. Shires[9], R. Silva Coutinho[48], G. Simi[22], M. Sirendi[47], N. Skidmore[46], I. Skillicorn[51], T. Skwarnicki[59], N. A. Smith[52], E. Smith[49,55], E. Smith[53], J. Smith[47], M. Smith[54], H. Snoek[41], M. D. Sokoloff[57], F. J. P. Soler[51], F. Soomro[39], D. Souza[46], B. Souza De Paula[2], B. Spaan[9], P. Spradlin[51],

S. Sridharan[38], F. Stagni[38], M. Stahl[11], S. Stahl[11], O. Steinkamp[40], O. Stenyakin[35], F Sterpka[59], S. Stevenson[55], S. Stoica[29], S. Stone[59], B. Storaci[40], S. Stracka[23,t], M. Straticiuc[29], U. Straumann[40], R. Stroili[22], L. Sun[57], W. Sutcliffe[53], K. Swientek[27], S. Swientek[9], V. Syropoulos[42], M. Szczekowski[28], P. Szczypka[38,39], T. Szumlak[27], S. T'Jampens[4], M. Teklishyn[7], G. Tellarini[16,f], F. Teubert[38], C. Thomas[55], E. Thomas[38], J. van Tilburg[41], V. Tisserand[4], M. Tobin[39], J. Todd[57], S. Tolk[42], L. Tomassetti[16,f], D. Tonelli[38], S. Topp-Joergensen[55], N. Torr[55], E. Tournefier[4], S. Tourneur[39], M. T. Tran[39], M. Tresch[40], A. Trisovic[38], A. Tsaregorodtsev[6], P. Tsopelas[41], N. Tuning[41], M. Ubeda Garcia[38], A. Ukleja[28], A. Ustyuzhanin[64], U. Uwer[11], C. Vacca[15,e], V. Vagnoni[14], G. Valenti[14], A. Vallier[7], R. Vazquez Gomez[18], P. Vazquez Regueiro[37], C. Vázquez Sierra[37], S. Vecchi[16], J. J. Velthuis[46], M. Veltri[17,h], G. Veneziano[39], M. Vesterinen[11], JVVB Viana Barbosa[38], B. Viaud[7], D. Vieira[2], M. Vieites Diaz[37], X. Vilasis-Cardona[36,p], A. Vollhardt[40], D. Volyanskyy[10], D. Voong[46], A. Vorobyev[30], V. Vorobyev[34], C. Voß[63], J. A. de Vries[41], R. Waldi[63], C. Wallace[48], R. Wallace[12], J. Walsh[23], S. Wandernoth[11], J. Wang[59], D. R. Ward[47], N. K. Watson[45], D. Websdale[53], M. Whitehead[48], D. Wiedner[11], G. Wilkinson[38,55], M. Wilkinson[59], M. P. Williams[45], M. Williams[56], H.W. Wilschut[66], F. F. Wilson[49], J. Wimberley[58], J. Wishahi[9], W. Wislicki[28], M. Witek[26], G. Wormser[7], S. A. Wotton[47], S. Wright[47], K. Wyllie[38], Y. Xie[61], Z. Xing[59], Z. Xu[39], Z. Yang[3], X. Yuan[3], O. Yushchenko[35], M. Zangoli[14], M. Zavertyaev[10,b], L. Zhang[3], W. C. Zhang[12], Y. Zhang[3], A. Zhelezov[11], A. Zhokhov[31], L. Zhong[3]

[1] Centro Brasileiro de Pesquisas Físicas (CBPF), Rio de Janeiro, Brazil
[2] Universidade Federal do Rio de Janeiro (UFRJ), Rio de Janeiro, Brazil
[3] Center for High Energy Physics, Tsinghua University, Beijing, China
[4] LAPP, Université de Savoie, CNRS/IN2P3, Annecy-Le-Vieux, France
[5] Clermont Université, Université Blaise Pascal, CNRS/IN2P3, LPC, Clermont-Ferrand, France
[6] CPPM, Aix-Marseille Université, CNRS/IN2P3, Marseille, France
[7] LAL, Université Paris-Sud, CNRS/IN2P3, Orsay, France
[8] LPNHE, Université Pierre et Marie Curie, Université Paris Diderot, CNRS/IN2P3, Paris, France
[9] Fakultät Physik, Technische Universität Dortmund, Dortmund, Germany
[10] Max-Planck-Institut für Kernphysik (MPIK), Heidelberg, Germany
[11] Physikalisches Institut, Ruprecht-Karls-Universität Heidelberg, Heidelberg, Germany
[12] School of Physics, University College Dublin, Dublin, Ireland
[13] Sezione INFN di Bari, Bari, Italy
[14] Sezione INFN di Bologna, Bologna, Italy
[15] Sezione INFN di Cagliari, Cagliari, Italy
[16] Sezione INFN di Ferrara, Ferrara, Italy
[17] Sezione INFN di Firenze, Florence, Italy
[18] Laboratori Nazionali dell'INFN di Frascati, Frascati, Italy
[19] Sezione INFN di Genova, Genoa, Italy
[20] Sezione INFN di Milano Bicocca, Milan, Italy
[21] Sezione INFN di Milano, Milan, Italy
[22] Sezione INFN di Padova, Padua, Italy
[23] Sezione INFN di Pisa, Pisa, Italy
[24] Sezione INFN di Roma Tor Vergata, Rome, Italy
[25] Sezione INFN di Roma La Sapienza, Rome, Italy
[26] Henryk Niewodniczanski Institute of Nuclear Physics Polish Academy of Sciences, Kraków, Poland
[27] Faculty of Physics and Applied Computer Science, AGH-University of Science and Technology, Kraków, Poland
[28] National Center for Nuclear Research (NCBJ), Warsaw, Poland
[29] Horia Hulubei National Institute of Physics and Nuclear Engineering, Bucharest-Magurele, Romania
[30] Petersburg Nuclear Physics Institute (PNPI), Gatchina, Russia
[31] Institute of Theoretical and Experimental Physics (ITEP), Moscow, Russia
[32] Institute of Nuclear Physics, Moscow State University (SINP MSU), Moscow, Russia
[33] Institute for Nuclear Research of the Russian Academy of Sciences (INR RAN), Moscow, Russia
[34] Budker Institute of Nuclear Physics (SB RAS) and Novosibirsk State University, Novosibirsk, Russia
[35] Institute for High Energy Physics (IHEP), Protvino, Russia
[36] Universitat de Barcelona, Barcelona, Spain
[37] Universidad de Santiago de Compostela, Santiago de Compostela, Spain

[38] European Organization for Nuclear Research (CERN), Geneva, Switzerland

[39] Ecole Polytechnique Fédérale de Lausanne (EPFL), Lausanne, Switzerland

[40] Physik-Institut, Universität Zürich, Zurich, Switzerland

[41] Nikhef National Institute for Subatomic Physics, Amsterdam, The Netherlands

[42] Nikhef National Institute for Subatomic Physics and VU University Amsterdam, Amsterdam, The Netherlands

[43] NSC Kharkiv Institute of Physics and Technology (NSC KIPT), Kharkiv, Ukraine

[44] Institute for Nuclear Research of the National Academy of Sciences (KINR), Kyiv, Ukraine

[45] University of Birmingham, Birmingham, UK

[46] H.H. Wills Physics Laboratory, University of Bristol, Bristol, UK

[47] Cavendish Laboratory, University of Cambridge, Cambridge, UK

[48] Department of Physics, University of Warwick, Coventry, UK

[49] STFC Rutherford Appleton Laboratory, Didcot, UK

[50] School of Physics and Astronomy, University of Edinburgh, Edinburgh, UK

[51] School of Physics and Astronomy, University of Glasgow, Glasgow, UK

[52] Oliver Lodge Laboratory, University of Liverpool, Liverpool, UK

[53] Imperial College London, London, UK

[54] School of Physics and Astronomy, University of Manchester, Manchester, UK

[55] Department of Physics, University of Oxford, Oxford, UK

[56] Massachusetts Institute of Technology, Cambridge, MA, USA

[57] University of Cincinnati, Cincinnati, OH, USA

[58] University of Maryland, College Park, MD, USA

[59] Syracuse University, Syracuse, NY, USA

[60] Pontifícia Universidade Católica do Rio de Janeiro (PUC-Rio), Rio de Janeiro, Brazil, associated to[2]

[61] Institute of Particle Physics, Central China Normal University, Wuhan, Hubei, China, associated to[3]

[62] Departamento de Fisica, Universidad Nacional de Colombia, Bogota, Colombia, associated to[8]

[63] Institut für Physik, Universität Rostock, Rostock, Germany, associated to[11]

[64] National Research Centre Kurchatov Institute, Moscow, Russia, associated to[31]

[65] Instituto de Fisica Corpuscular (IFIC), Universitat de Valencia-CSIC, Valencia, Spain, associated to[36]

[66] Van Swinderen Institute, University of Groningen, Groningen, The Netherlands, associated to[41]

[67] Celal Bayar University, Manisa, Turkey, associated to[38]

[a] Universidade Federal do Triângulo Mineiro (UFTM), Uberaba, MG, Brazil

[b] P.N. Lebedev Physical Institute, Russian Academy of Science (LPI RAS), Moscow, Russia

[c] Università di Bari, Bari, Italy

[d] Università di Bologna, Bologna, Italy

[e] Università di Cagliari, Cagliari, Italy

[f] Università di Ferrara, Ferrara, Italy

[g] Università di Firenze, Florence, Italy

[h] Università di Urbino, Urbino, Italy

[i] Università di Modena e Reggio Emilia, Modena, Italy

[j] Università di Genova, Genoa, Italy

[k] Università di Milano Bicocca, Milan, Italy

[l] Università di Roma Tor Vergata, Rome, Italy

[m] Università di Roma La Sapienza, Rome, Italy

[n] Università della Basilicata, Potenza, Italy

[o] Faculty of Computer Science, Electronics and Telecommunications, AGH-University of Science and Technology, Kraków, Poland

[p] LIFAELS, La Salle, Universitat Ramon Llull, Barcelona, Spain

[q] Hanoi University of Science, Hanoi, Vietnam

[r] Università di Padova, Padua, Italy

[s] Università di Pisa, Pisa, Italy

[t] Scuola Normale Superiore, Pisa, Italy

[u] Università degli Studi di Milano, Milan, Italy

[v] Politecnico di Milano, Milano, Italy